Ferromagnesian postperovskite silicates in the D″ layer of the Earth

Wendy L. Mao*†‡, Guoyin Shen§, Vitali B. Prakapenka§, Yue Meng¶, Andrew J. Campbell*, Dion L. Heinz*‖, Jinfu Shu†, Russell J. Hemley†, and Ho-kwang Mao*†¶‖

*Department of the Geophysical Sciences, University of Chicago, 5734 South Ellis Avenue, Chicago, IL 60637; †Geophysical Laboratory, Carnegie Institution of Washington, 5251 Broad Branch Road NW, Washington, DC 20015; §Consortium for Advanced Radiation Sources and ‖James Franck Institute, University of Chicago, 5640 South Ellis Avenue, Chicago, IL 60637; and ¶High-Pressure Collaborative Access Team, Advanced Photon Source, Argonne National Laboratory, 9700 South Cass Avenue, Argonne, IL 60439

Contributed by Ho-kwang Mao, September 28, 2004

Natural olivine with 12 mol % Fe_2SiO_4 and synthetic orthopyroxenes with 20% and 40% $FeSiO_3$ were studied beyond the pressure–temperature conditions of the core–mantle boundary. All samples were found to convert entirely or partially into the $CaIrO_3$ postperovskite structure, which was recently reported for pure $MgSiO_3$. The incorporation of Fe greatly reduces the pressure needed for the transition and establishes the new phase as the major component of the D″ layer. With the liquid core as an unlimited reservoir of iron, core–mantle reactions could further enrich the iron content in this phase and explain the intriguing seismic signatures observed in the D″ layer.

The D″ boundary layer between the crystalline silicate mantle and molten Fe core displays the largest contrast in physical and chemical properties of all of the regions in the Earth and undoubtedly plays a pivotal role in global dynamics and evolution (1–4). Recent high pressure–temperature (*P-T*) experiments (5, 6) and *ab initio* theoretical calculations (6–8) indicate that the pure end-member $MgSiO_3$ transforms to a postperovskite (ppv) phase with the $CaIrO_3$ structure. The relevance of this new phase to the Earth's interior, however, depends on its stability within the physical–chemical boundary conditions of the D″ layer. For instance, Murakami *et al.* (5) observed this transition at 125 GPa and 2,500 K, which is still within the *P-T* limits of the D″ layer (<136 GPa). On the other hand, Shim *et al.* (9) observed the x-ray diffraction pattern of modified $MgSiO_3$ perovskite (pv) (9) persisting to higher *P* (144 ± 10 GPa), and additional peaks consistent with ppv occur only after heating to 2,500 K at 144 GPa, i.e., beyond the limit of the D″ layer. More importantly, the D″ layer is in contact with an unlimited source of Fe and possibly FeO in the outer core, and its major phases are dictated by the Fe-rich environment. Does Fe enter the ppv structure? Is the ppv phase stabilized or destabilized by the addition of Fe? Could the Fe content in ppv phase be enriched beyond the mantle ferromagnesian silicate compositions? How does the Fe concentration affect the density buoyancy and thermoelasticity of the ppv phase?

Besides shock-wave studies (10), direct experiment on relevant ferromagnesian silicate compositions have never been carried out at the *P-T* conditions of the D″ layer. We studied three ferromagnesian silicates in diamond anvil cells to 130–165 GPa with laser heating to 2,500 K and observed the transformation to ppv phase in all three samples. The starting materials are two synthetic orthopyroxenes with chemical molar compositions of $(Mg_{0.8}Fe_{0.2})SiO_3$ (En80) and $(Mg_{0.6}Fe_{0.4})SiO_3$ (En60), and San Carlos olivine with the composition of $(Mg_{0.88}Fe_{0.12})_2SiO_4$. Experiments were conducted at the 13IDD beamline of the GeoSoilEnviro Consortium for Advanced Radiation Sources and the 16IDB beamline of the High-Pressure Collaborative Access Team at Argonne National Laboratory; both beamlines are optimized for monochromatic x-ray diffraction study of high-*P* samples with *in situ* laser heating (11, 12). The silicate sample was sandwiched between thin layers of NaCl, which served as thermal insulation during laser heating and as the pressure calibrant (13), placed in a 40-μm-diameter sample chamber in a rhenium gasket in a symmetrical diamond anvil cell, raised to specific pressures, heated with yttrium lithium fluoride lasers from both sides, and monitored with x-ray diffraction *in situ* at high *P-T* and at ambient *T* and high *P* after temperature quench.

Table 1. hkl reflections for the ppv phase used in unit cell determination for En80 taken at 108 GPa and San Carlos olivine at 144 GPa at 300 K after *T* quench from 2,000 K

	En80 *d*-spacing, Å		San Carlos olivine *d*-spacing, Å	
hkl	Observed	Calculated	Observed	Calculated
020	4.067	4.065	3.990	3.991
002	3.061	3.059	3.034	3.036
022	2.443	2.444	2.413	2.416
110	—	—	2.336	2.335
023	1.821	1.823	1.802	1.805
131	1.747	1.749	1.722	1.725
132	1.568	1.568	1.548	1.548
113	1.544	1.544	1.531	1.529
004	1.529	1.529	1.518	1.518
043	1.437	1.440	1.422	1.421
062*	1.239	1.239	1.219	1.219
044	1.223	1.222	1.208	1.208

Observed *d*-spacings were used to fit lattice parameters; the *d*-spacings calculated from those lattice parameters are given for comparison.
*The 062 peak contains contributions from the 152, 062, and 200 reflections.

For two of the samples, we took a direct path to the synthesis conditions by compressing the starting materials at ambient *T* to the maximum *P* and then laser-heating the highly metastable, pressure-amorphized initial phases. En80 was first compressed to 108 GPa. The x-ray diffraction image showed a broad amorphous background without distinctive peaks. Then, the sample was heated to 2,000 K at high *P*. Within 2 min, 11 diffraction peaks corresponding to the ppv phase appeared together with several peaks of pv, indicating the presence of a pv + ppv two-phase region (Figs. 1 and 2). The unit cell parameters for the ppv phase at 108 GPa and 300 K after *T* quench were a = 2.470(4) Å, b = 8.130(6) Å, and c = 6.117(4) Å (Table 1). These values correspond to a ferromagnesian ppv silicate $(Fe_xMg_{1-x})SiO_3$ with x slightly over 0.2 (Fig. 3).

San Carlos olivine was compressed to 150 GPa and heated to 2,000 K. The sample decomposed completely to ppv + magnesiowüstite (mw) without any observable pv (Fig. 2). The unit cell

Abbreviations: mw, magnesiowüstite; ppv, postperovskite; pv, perovskite; *P*, pressure; *T*, temperature.

‡To whom correspondence should be addressed at the * address. E-mail: wmao@uchicago.edu.

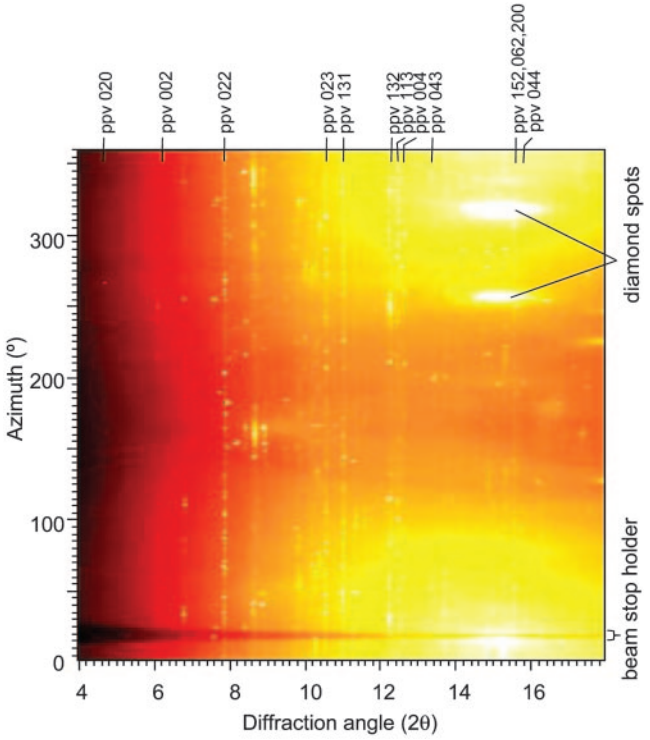

Fig. 1. Two-dimensional x-ray diffraction image of En80 at 108 GPa and 300 K after laser-heating to 2,000 K showing azimuthal angle versus 2θ. The large diamond spots are a result of single-crystal diffraction from the diamond anvils and were masked for the azimuthal integration of the spectra.

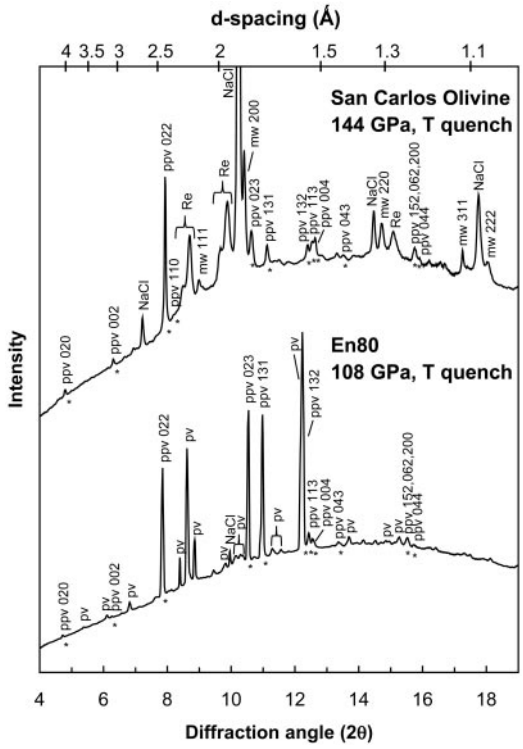

Fig. 2. X-ray diffraction patterns of En80 at 108 GPa and San Carlos olivine at 144 GPa. Both were taken at 300 K after laser-heating to 2,000 K. ppv peaks are marked with *. The San Carlos olivine spectra shows that the sample had converted to only ppv + mw phases. Splitting of the Re 100 and 101 peaks may be a result of repeated temperature cycling that transformed the edge of the gasket material into a double hexagonal close-packed (hcp) structure [similar to behavior observed in Fe and Co (21, 22)] or a hcp phase reaction product. The En80 sample shows conversion of the amorphized sample into ppv + pv. The ppv 132 peak is on the short-wavelength shoulder of a pv peak. The wavelength of the monochromatic beam was 0.3344 Å.

parameters of the ppv phase at 144 GPa and 300 K after T quench were $a = 2.442(2)$ Å, $b = 7.983(4)$ Å, and $c = 6.071(3)$ Å (Table 1). The cubic unit cell edge, $a = 3.687(2)$ Å, of the coexisting mw was close to that of pure MgO at the same pressure, indicating a preferred partitioning of Fe into ppv. This finding is in contrast to the Fe partitioning between pv and mw, which strongly favors mw (14).

We also conducted experiments along a stepwise path by first converting the sample to an intermediate assemblage at lower P. En60 was compressed to 40 GPa, laser-heated for 10 min, and converted to the known three-phase assemblage of pv + mw + stishovite (st) at this pressure (14, 15). The processes were repeated stepwise at pressure increments of 5–10 GPa. At 100 GPa, new diffraction lines corresponding to ppv appeared. Upon further pressure increments and repeated heating, the ppv diffraction peaks grew in intensity, but the coexisting pv + mw + st phases persisted to the maximum P of 160 GPa after 20 min of heating to 2,500 K. The results indicate that although the En60 ppv is stable above 100 GPa, the reaction kinetics from pv are very sluggish. This finding could explain the pv to 144 GPa observed by Shim *et al.* (9) and the persistence of pv in the stability field of ppv observed by Murakami *et al.* (5). In both experiments, ppv was converted from pv. Moreover, the reaction kinetics between pv and ppv is much lower at decreasing temperatures. This uncertainty prevents us from determination of the Clapeyron slope at the present stage. Multiple experiments of the aforementioned direct path from olivine and pyroxene would be required for determination of the slope in the future.

We demonstrate that a larger amount of oxidized Fe can be incorporated in the ppv than in any other known lower mantle silicate phase, that Fe preferentially enters ppv relative to pv and possibly mw, and that Fe can stabilize the ppv phase at appreciably lower P than that required for the pure $MgSiO_3$ end member. A schematic phase diagram is presented in Fig. 3. The present observation has enormous implications for developing the new paradigm for the D″ layer (4). For instance, we could

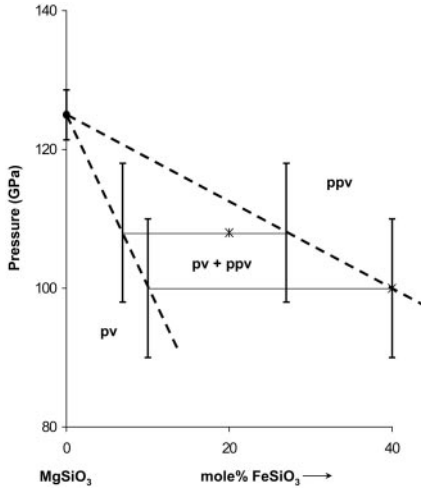

Fig. 3. Schematic phase diagram of the $MgSiO_3$–$FeSiO_3$ binary system at 2,000–2,500 K. Depending on the temperature at the core–mantle boundary, the phase boundaries could shift upward by 10–20 GPa based on a positive Clapeyron slope (5, 6).

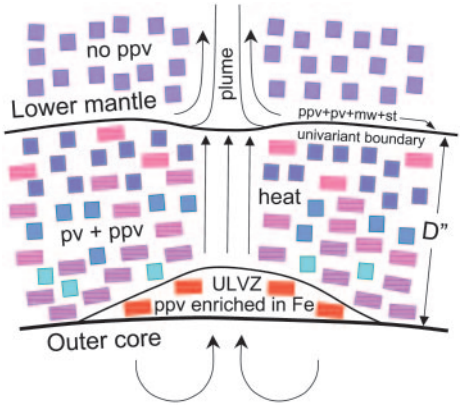

Fig. 4. Schematic cross section of the D″ zone. The shading in the squares (pv) and striped rectangles (ppv) reflects the changing Fe/Mg ratio, with an increasing red color indicating higher Fe content in that phase. The Fe/Mg and pv/ppv ratio follows the two phase loops in the phase diagram.

make the following speculations. The sharp D″ discontinuity could represent the pv + st + mw ↔ pv + ppv univariant phase boundary, and the mild, negative velocity gradient within D″ could represent Fe–Mg equilibration along the broad pv + ppv two-phase loop in the *P-T-x* space. Hotter regions at the base of D″ then promote strong local interaction with the outer core and add a large amount of Fe into the ferromagnesian ppv silicate, thus producing ultra-low-velocity zones (ULVZ) by increasing the mean atomic number of the silicate. These ULVZ may also represent heat sources for plumes resulting in the observed hot spots (16–20). The addition of Fe may also affect the elastic anisotropy of ferromagnesian ppv silicate, which would have implications to its representing the source of the S-wave splitting in D″. A full understanding of the implications of ferromagnesian ppv silicate to the core–mantle boundary layer awaits the detailed characterization of its physical and chemical properties in the relevant *P-T-x* space, but the emerging paradigm is that the D″ layer may be mainly a phase transition zone of ferromagnesian silicates and a reaction zone between the Fe core and silicate mantle (Fig. 4).

We thank Professor D. H. Lindsley (State University of New York, Stony Brook) for the two synthetic orthopyroxene starting materials and the GeoSoilEnviro Consortium for Advanced Radiation Sources (GSECARS), the High-Pressure Collaborative Access Team (HPCAT), and the Advanced Photon Source for synchrotron beam time. GSECARS is supported by National Science Foundation (NSF) Earth Sciences (EAR) Grant EAR-0217473, Department of Energy (DOE) Geosciences Grant DE-FG02-94ER14466, and the State of Illinois. HPCAT is supported by the DOE Basic Energy Sciences (BES), the DOE–National Nuclear Security Administration Carnegie/DOE Alliance Center, the NSF, the Department of Defense–Tank-Automotive and Armament Command, and the W. M. Keck Foundation. Use of the Advanced Photon Source was supported by the DOE-BES, Office of Energy Research, under Contract W-31-109-Eng-38. This work was supported by the NSF-EAR Geochemistry, NSF-EAR Geophysics 0309486, and NSF-EAR Instrumentation and Facility programs.

1. Sidorin, I., Gurnis, M. & Helmberger, D. V. (1999) *Science* **286,** 1326–1331.
2. Lay, T., Williams, Q. & Garmerp, E. J. (1998) *Nature* **392,** 461–468.
3. Anderson, D. L. (1998) in *The EDGES of the Mantle*, eds. Gurnis, M., Wysession, M. E., Knittle, E. & Buffett, B. A. (Am. Geophys. Union, Washington, DC), pp. 255–271.
4. Garnero, E. J. (2004) *Science* **304,** 834–836.
5. Murakami, M., Hirose, K., Kawamura, K., Sata, N. & Ohishi, Y. (2004) *Science* **304,** 855–858.
6. Oganov, A. R. & Ono, S. (2004) *Nature* **430,** 445–448.
7. Iitaka, T., Hirose, K., Kawamura, K. & Murakami, M. (2004) *Nature* **430,** 442–445.
8. Tsuchiya, T., Tsuchiya, J., Umemoto, K. & Wentzcovitch, R. M. (July 17, 2004) *Geophys. Res. Lett.* **31,** 10.1029/2004GL020278.
9. Shim, S.-H., Duffy, T. S., Jeanloz, R. & Shen, G. (May 18, 2004) *Geophys. Res. Lett.* **31,** 10.1029/2004GL019639.
10. Luo, S.-N., Mosenfelder, J. L., Asimow, P. D. & Ahrens, T. J. (July 25, 2002) *Geophys. Res. Lett.* **29,** 10.1029/2002GL015627.
11. Ming, L. C. & Bassett, W. A. (1974) *Rev. Sci. Instrum.* **45,** 1115–1118.
12. Shen, G., Rivers, M. L., Wang, Y. & Sutton, S. R. (2001) *Rev. Sci. Instrum.* **72,** 1273–1282.
13. Sata, N., Shen, G., Rivers, M. L. & Sutton, S. R. (2002) *Phys. Rev. B* **65,** 104114.
14. Mao, H. K., Shen, G. & Hemley, R. J. (1997) *Science* **278,** 2098–2100.
15. Mao, H. K., Yagi, T. & Bell, P. M. (1977) *Year Book Carnegie Inst. Washington* **76,** 502–504.
16. Montelli, R., Nolet, G., Dahlen, F. A., Masters, G., Engdahl, E. R. & Hung, S.-H. (2004) *Science* **303,** 338–343.
17. Helmberger, D. V., Ni, S., Wen, L. & Ritsema, J. (2000) *J. Geophys. Res.* **105,** 23865–23878.
18. Helmberger, D. V., Wen, L. & Ding, X. (1998) *Nature* **396,** 251–255.
19. Wen, L. & Helmberger, D. V. (1998) *Science* **279,** 1701–1703.
20. Williams, Q., Revenaugh, J. & Garnero, E. (1998) *Science* **281,** 546–549.
21. Yoo, C. S., Soderlind, P. & Cynn, H. (1998) *J. Phys. Condens. Matter* **10,** L311.
22. Yoo, C. S., Soderlind, P., Moriarty, J. & Campbell, A. (1996) *Phys. Lett. A* **214,** 65–70.